Article

Enhancing Cytochrome C Recognition and Adsorption through Epitope-Imprinted Mesoporous Silica with a Tailored Pore Size

Dandan Cheng, Xin Han, Jiawen Zou, Zhenyu Li, Meiru Wang, Yuqing Liu, Kexuan Wang, and Yan Li*

Cite This: ACS Omega 2024, 9, 1134−1142

Read Online

ACCESS | Metrics & More | Article Recommendations | SI Supporting Information

ABSTRACT: We have reported the synthesis of epitope-imprinted mesoporous silica (EIMS) with an average pore size of 6.2 nm, which is similar to the geometrical size of the target protein, cytochrome C (Cyt c, $2.6 \times 3.2 \times 3.3$ nm^3), showing great recognition and large-scale adsorption performance. The characteristic fragment of Cyt c was used as a template and docked onto the surface of C_{16}MIMCl micelles via multiple interactions. Nitrogen adsorption−desorption and transmission electron microscopy confirmed the successful preparation of EIMS. Due to the ordered pore structure, larger pore size, and high specific surface area, the prepared EIMS show superior specificity (IF = 3.8), excellent selectivity toward Cyt c, high adsorption capacity (249.6 mg g^{-1}), and fast adsorption equilibrium (10 min). This study demonstrates the potential application of EIMS with a controllable pore size for high-effective and large-scale separation of Cyt c, providing a new approach for effective biomacromolecular recognition.
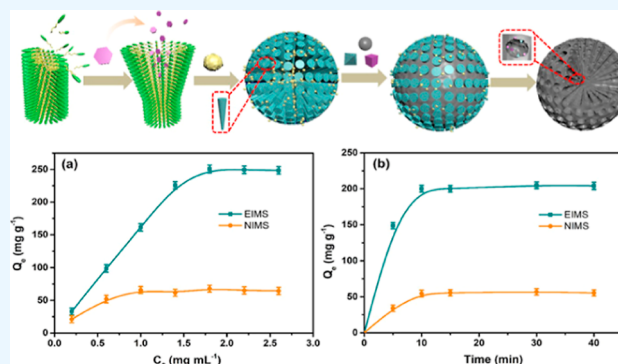
1. INTRODUCTION

Cytochrome C (Cyt c) is a water-soluble heme protein, which can be used in the first aid or auxiliary treatment of various tissue hypoxia, such as oxidized carbon and hypnotic poisoning, neonatal asphyxia, brain trauma, and other causes of brain hypoxia.[1−5] It also ameliorates leukocyte reduction, limb circulation disorder, liver disease, and nephritis caused by anticancer drugs.[6] Cyt c is usually extracted from pig or cow heart tissues, which are complex biological sample matrices.[6] Considering that the functions of proteins are closely related to their special conformations and bioactivities, it is therefore highly desirable to develop environment-friendly and biocompatible adsorbents in order to maintain the conformation and activity of protein species during the solid-phase extraction process.[6−8] Besides, the selective adsorption for specific proteins of interest under controlled experimental conditions is required for the biocompatible adsorbents. Molecular imprinting technology using an appropriate adsorbent is among the widely employed alternatives for protein separation and preconcentration, which has the advantages of high efficiency, relatively low running cost, easy automatic operation, as well as the absence of toxic organic solvents.[2−6]

However, protein imprinting remains challenging due to its low imprinting efficiency and poor specificity. During the imprinting process, fragile template proteins tend to suffer severe conformational changes under available polymerization conditions.[5] Moreover, since a large portion of proteins is buried in the highly cross-linked polymer networks, it is very difficult to remove them and generate imprinting cavities with high fidelity. Epitope imprinting, which utilizes smaller and more rigid characteristic peptides as pseudotemplates, is a promising strategy to avoid these related issues.[6−9] For example, Nishino et al. utilized the C-terminal nonapeptides (residues 96−104, AYLKKATNE, residues 599−607, VVSTQTALA, residues 339−347, GRYVVDTSK) as imprinted templates for selectively isolating and purifying bovine serum album (BSA), alcohol dehydrogenase, and Cyt c, respectively.[10] Notably, during the recognition process, excellent accessibility of imprinted sites to target proteins is needed and therefore surface imprinting technology is combined.[11] Accordingly, the supporting matrix for surface-imprinted materials should be well designed for a satisfactory adsorption capacity and flexible mass transfer.

Mesoporous silica is a kind of appropriate supporting matrix featuring well-ordered pore structure, high surface area and adjustable pore size.[12−14] Docking oriented imprinting is usually achieved within mesoporous silica by preanchoring the templates along the periphery of micellar rods, followed by one-step sol−gel synthesis. After the elution of templates and pore-forming micelles, the recognition sites toward templates

would be confined on the surface of mesoporous channel and thereby offer high accessibility for recombination.[15] Thereinto, it is urgent to develop a kind of surfactant, which could not only form micelles but also provide multiple interactions (such as electrostatic, hydrogen bonding, $\pi-\pi$ stacking interaction, van der Waals interactions, etc.) to mediate the preassembly of templates and micelles.[16−19] In view of that, amphiphilic ionic liquids (ILs) have gradually found wide applications as special surfactants for their tunable structures and properties.[20−23] For example, Ding et al. synthesized hexapeptide-imprinted mesoporous silica by using 1-dodecyl-3-methylimidazolium chloride (C_{12}MIMCl) as the surfactant and the corresponding imprinting factor (IF) could reach up to 4.51.[24] Meanwhile, Li et al. reported the utilization of 1-octadecyl-3-methylimidazolium chloride (C_{18}MIMCl) as surfactant and the formed pore size was 3.62 nm.[25] Although the combination of oriented docking and epitope surface imprinting holds great promise, target proteins with large size still face obstacles of going in/out of the channel.[26,27]

Several methods are proposed to enlarge the pore size of mesoporous imprinted materials.[28−30] Conventional oil-based synthesis systems use a large number of oil phases to achieve an effective swelling effect. In the anion-assisted method, salicylic acid anion (Sal^-) is used to form large pores, and the amount required is significantly reduced, indicating that Sal^- has superior micellar penetration compared to the oil phase.[31,32] The strong interaction between Sal^- and CTA^+ micelles, including high miscibility and strong electrostatic attraction, drives Sal^- to migrate into the micelles, and its hydrophobic part is embedded in the hydrophobic region of the micelles.[33−36] Therefore, the anion-assisted method is highly reproducible and the effect of the stirring rate on the particle structure is negligible.[36] In contrast, nonpolar oil molecules lack attraction to the hydrophobic nuclei of micelles.[37] In addition, oil molecules in oil/water suspensions tend to form large oil clumps. Therefore, it is of great significance for introducing organic auxiliaries into amphiphilic IL micelles to obtain satisfactory protein-mass transfer channels.

Herein, according to Figure 1, sodium salicylate (NaSal) was utilized as an auxiliary of an amphiphilic IL (C_{16}MIMCl) to form expanded composite micelles. Subsequently, nonapeptide as an epitope of Cyt c was anchored onto the surface of

Figure 1. Preparation procedure of epitope imprinted mesoporous silica.

expanded composite micelles through multiple interactions. After that, a mixture of tetraethoxysilane (TEOS), 1-propyltrimethoxysilane-3-methylimidazolium chloride (PTES-MIC), and 3-aminopropyl trimethoxysilane (APTES) was introduced to form mesoporous imprinted materials (EIMS). The static/dynamic adsorption behavior and specific recognition performance of EIMS for Cyt c were studied systematically and the advantages over other recognition materials were illustrated.

2. EXPERIMENTS

2.1. Chemicals and Materials. Sodium salicylate (NaSal), triethanolamine (TEA, 85%), 1-chlorohexadecane, and 1-methylimidazole were provided by Macklin (Shanghai, China). Hydrochloric acid (36.0%), methanol, tetrahydrofuran (THF), and ethanol were obtained from Kermel (Tianjin, China). 1-PTESMIC, APTES, and TEOS were provided by Aladdin (Shanghai, China). Cyt c (M_w = 12.4 kDa) was purchased from Macklin (Shanghai, China). Lysozyme (Lyz, M_w = 13.4 kDa) and Ovalbumin (OVA, M_w = 45.0 kDa) were provided by Kangbeibio (Ningbo, China). Hemoglobin (Hb, M_w = 64.0 kDa) and BSA (M_w = 67.0 kDa) were purchased from Sigma-Aldrich. The C-terminal fragment of Cyt c (residues 96−104, AYLKKATNE) was synthesized by Apeptide (Shanghai, China).

2.2. Synthesis of Amphiphilic IL Surfactant C_{16}MIMCl. To synthesize amphiphilic IL (C_{16}MIMCl), equimolar amounts of 1-chlorohexadecane and 1-methylimidazole were added into a round-bottom flask and subjected to reflux at 90 °C for 24 h.[38] Then, the resulting product was purified through recrystallization in THF, followed by drying under a vacuum at 25 °C. The final product, C_{16}MIMCl, was characterized by ^{1}HNMR and Fourier transform infrared (FTIR) spectra.

2.2.1. Preparation of EIMS. First, C_{16}MIMCl (1.52 g) and ultrapure water (288 mL) were introduced into a round-bottom flask. After stirring for 15 min at 40 °C, the stable micelles were formed. Then, sodium salicylate (0.67 g) was added to micelles solution and the expanded composite micelles could be obtained by further reaction for 15 min. TEA (0.27 g) and deionized water (100 mL) were introduced into a flat-bottomed flask with magnetic stirring for 0.5 h at 80 °C. Subsequently, TEA (0.27 g) was introduced to make the above solution alkaline, which facilitated the hydrolysis of TEOS. After stirring uniformly, template nonapeptide (0.15 g) was introduced and the solution was stirred for 10 min. What is more, PTESMIC (0.38 g), APTES (1.2 mL), and TEOS (25 mL) were added dropwise to the mixture solution and the reaction was continued under stirring for 24 h to obtain the white precipitate. The product was obtained after filtration and washed several times with ultrapure water, followed by Soxhlet extraction to remove the expanded composite micelles and nonapeptide. Thereafter, the product was vacuum-dried at 40 °C to obtain EIMS. The preparation of nonimprinted mesoporous silica (NIMS) was identical to EIMS except for the absence of the template nonapeptide.

2.3. Isothermal Rebinding and Dynamic Adsorption. To investigate the adsorption behavior of EIMS toward Cyt c, dried EIMS and NIMS were added into phosphate buffer solution (PBS, pH 7.4, 5 mL) containing varying concentrations of Cyt c (ranging from 0.2 to 2.6 mg mL^{-1}). The mixture was incubated with shaking at room temperature for 24 h, followed by filtration through a 0.1 μm poly(ether sulfone) syringe filter to accurately determine the concen-
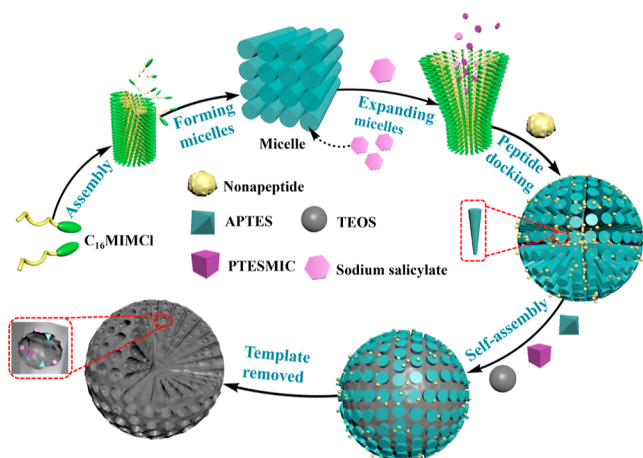
tration of Cyt *c* in the supernatant. Adsorption kinetics tests were conducted by incubating 30 mg of dried EIMS and NIMS in PBS solution (pH 7.4, 5 mL) containing 1.8 mg mL^{-1} of Cyt *c* at 25 °C for different time intervals and subsequently measuring the concentration of residual Cyt *c* solution by UV−vis spectrum. IF, an important index for evaluating the selectivity of imprinted polymers, can be calculated using formula 1 through obtaining the adsorption capacities of EIMS (Q_{EIMS}) and NIMS (Q_{NIMS}) for Cyt *c*.

$$IF = \frac{Q_{EIMS}}{Q_{NIMS}} \qquad (1)$$

2.4. Selectivity and Competitive Adsorption Experiments. To evaluate the selectivity of EIMS for Cyt *c*, 30 mg of dried EIMS and NIMS were incubated in freshly prepared PBS solution (pH 7.4, 5 mL) containing 1.8 mg mL^{-1} of Cyt *c* and other proteins (BSA, OVA, Hb, Lyz) for 24 h at 25 °C with gentle shaking. The residual concentrations of these proteins were determined by UV−vis spectrum to obtain the amount of each protein adsorbed by EIMS and NIMS. The selectivity coefficient (β) was calculated using eqn S3 (Supporting Information) to assess the specificity of EIMS toward Cyt *c*. Competition experiments were performed by adding 30 mg of EIMS (NIMS) into PBS solution (pH 7.4, 5 mL) containing a protein mixture of Cyt *c* and its competitors (BSA, OVA) at a concentration of 1.8 mg mL^{-1}. After incubation for 24 h at 25 °C with gentle shaking, EIMS and NIMS were treated with PBS solution containing 5 mM NaCl (pH 7.4) to remove the nonspecifically adsorbed protein. The specifically adsorbed proteins were eluted using 0.5 M NaCl solution and processed using dialysis tubing with a molecular cutoff of 500 Da to remove residual NaCl. The obtained protein was dissolved in PBS solution (pH 7.4, 5 mL), and 10 μL of the solution was analyzed by sodium dodecyl sulfate−polyacrylamide gel electrophoresis (SDS−PAGE) using a 12.5% polyacrylamide separating gel and 5% polyacrylamide stacking gel to determine the extent of protein adsorption.[39]

2.5. Reusability. The reusability adsorption experiments were performed five times at 25 °C using the same batches of EIMS. Thirty mg of EIMS and NIMS were respectively placed in Cyt *c* PBS solution (5 mL, 1.8 mg mL^{-1}, pH 7.4) for 24 h, and then, the solution was centrifuged at 5500 rpm for 10 min. The concentration of Cyt *c* residue was determined by the UV spectrum to acquire the amount of adsorbed Cyt *c*. Finally, EIMS were eluted to remove Cyt *c* and further reused in the subsequent adsorption−desorption cycles.

2.6. Characterization. ^{1}H NMR spectra of C$_{16}$MIMCl were acquired with Bruker AVANCE at 400 MHz using CDCl$_{3}$ as the solvent and tetramethylsilane as an internal standard. FTIR spectra (4000−500 cm^{-1}) was collected on TENSOR27 FTIR spectrometer (Bruker). The morphologies of EIMS and NIMS were determined by SEM (Verios G4) and TEM (Talos F200X G2). The specific surface area and pore size distribution of EIMS and NIMS were measured by a BET (3H-2000PS2). Zeta potentials of Cyt *c*, EIMS, and NIMS over a wide pH range were measured by zeta potential measurement (ZetaPlus, Bruker) to define the surface electrification property and iso-electric point (IEP). UV-2550 spectrophotometer (Shimadzu, Japan) was used to confirm the concentration of the biomolecule solution. SDS−PAGE was conducted by utilizing a DYY-6C electrophoresis system (Beijing Liuyi Instrument Plant, China).

3. RESULTS AND DISCUSSION

3.1. Characterization of Amphiphilic IL C$_{16}$MIMCl. The ^{1}HNMR (Figure S1) and FTIR (Figure S1) spectra are used to confirm the structure of C$_{16}$MIMCl. As shown in Figures S1 and S2, the chemical signals generated by the functional groups and the chemical shifts of H in amphiphilic IL (C$_{16}$MIMCl) can be found in FT-IR spectra and ^{1}HNMR spectrum, respectively, suggesting that the amphiphilic IL (C$_{16}$MIMCl) is successfully synthesized.

3.2. Morphology and Structure Characterization of EIMS and NIMS. Except for the addition of template nonapeptide to the synthesis of EIMS, the synthesis process of EIMS and NIMS is almost the same and the template nonapeptide is eluted after the preparation of EIMS. Therefore, the chemical structure of EIMS and NIMS should be the same and can be characterized by the FTIR spectrum. The FTIR spectrum of EIMS in Figure 2 shows that the
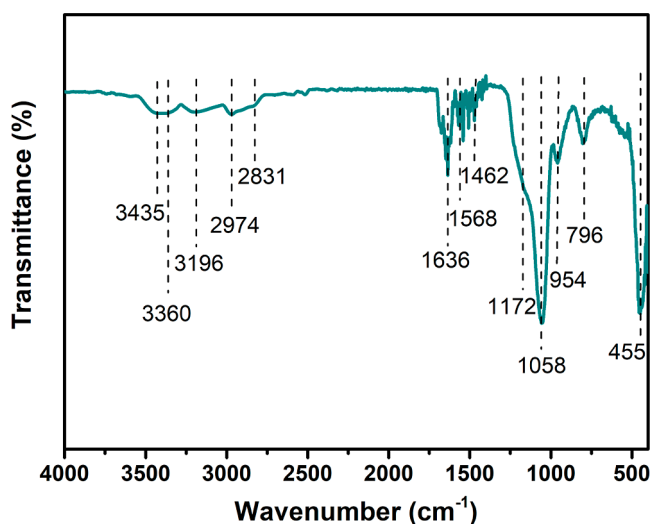

Figure 2. FTIR spectrum of EIMS.

absorption peaks at 1636, 1058, 954, 796, and 455 cm^{-1} are attributed to the bending vibration of Si−O−H, asymmetric stretching vibration of Si−O, symmetric stretching vibration of Si−O−H, symmetric stretching vibration of Si−O−Si and bending vibration of Si−O−Si respectively, indicating the successful synthesis of mesoporous silica by hydrolyzation-condensation of TEOS. The absorption peaks related to the stretching vibration of C−H on the imidazolium ring at 3360 and 3196 cm^{-1}, vibration of imidazole skeleton at 1568 cm^{-1}, and stretching vibration of the imidazolium ring at 1172 cm^{-1} can confirm the existence of PTESMIC in EIMS and NIMS. Besides, the absorption peaks related to the stretching vibration of C−H of −CH$_{2}$ and −CH$_{3}$ at 2974 and 2831 cm^{-1}, and the deformation vibration of −CH$_{3}$ at 1462 cm^{-1} provide evidence for the existence of APTES.

The TEM in Figure 3 shows that EIMS and NIMS are nearly spherical, with an average size of 200 nm. Moreover, ordered mesopores are observed for both microspheres. The specific surface area and pore-size distribution of EIMS/NIMS are shown in Figure 4, specifically, the Brunauer−Emmett−Teller surface area and the average pore size are 540.1 m^{2} g^{-1} and 6.2 nm for EIMS, while they are 772.0 m^{2} g^{-1} and 4.8 nm for NIMS. The smaller surface area of EIMS can be due to the extended pore size decreasing the pore number. EIMS show a
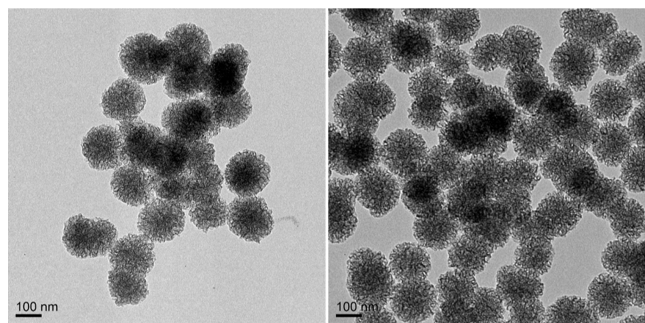
Figure 3. TEM images of EIMS (a) and NIMS (b).

slightly larger pore size than that of NIMS, which is attributed to that the imprinted cavities embedded on the surface of mesoporous channel of EIMS result in a further expansion of mesopores. In addition, the average pore size of EIMS (6.2 nm) is bigger than the overall size of Cyt c (2.6 × 3.2 × 3.3 nm^3), illustrating that there is a sufficient space for Cyt c recognition.

To verify the positive effect of the sodium salicylate auxiliaries, the pore size of EIMS and other reported imprinted mesoporous materials is summarized in Table 1.[40−42] Due to the addition of salicylic acid anion (Sal$^-$), the pore size of EIMS is increased significantly, and this design is conducive for improving the adsorption and recognition performance of EIMS.

3.3. Adsorption Properties of EIMS and NIMS. The rebinding isotherm and kinetics of EIMS/NIMS for Cyt c are systematically studied. As shown in Figure 5a, when the initial concentration of Cyt c reaches 1.8 mg mL^{-1}, the Cyt c adsorption of EIMS becomes saturated, while NIMS reaches adsorption equilibrium at the initial Cyt c concentration of 1.0 mg mL^{-1}. Langmuir isotherm model gives a better fit than that of the Freundlich isotherm model (Table 2, eqs S1 and S2), suggesting that the static adsorption of EIMS/NIMS toward Cyt c is more consistent with monolayer adsorption with the same active sites and energies. The maximum adsorption capacity of EIMS is calculated to be 249.6 mg g^{-1}, while for NIMS it is 65.6 mg g^{-1}, the corresponding IF is 3.8. Compared with previous work, the Cyt c adsorption capacity is increased by nearly three times and the IF is also increased from 3.5 to 3.8.[25] The results indicate that the expansion of pore size could facilitate more target proteins entering the channels easily to improve the adsorption capacity and imprinting efficiency.

Table 1. Comparison of Pore Sizes of Imprinted Mesoporous Materials[a]

carrier	template	pore-forming agent	pore-size (nm)	ref
mesoporous silica	AMP	CTAB	2.3	40
mesoporous silica	nonapeptide	C$_{18}$MIMCl	3.6	25
mesoporous silica	IHHC	C$_{12}$MIMCl	2.5	24
mesoporous silica	sparfloxacin	CTAB	3.1	41
mesoporous TiO$_2$	atrazine	P123	4.7	42
mesoporous silica	nonapeptide	C$_{16}$MIMCl	6.2	this method

[a]Note that adenosine monophosphate, immunostimulating hexapeptide from human casein (IHHC), cetyltrimethylammonium bromide, 1-octadecyl-3-methylimidazolium chloride (C$_{18}$MIMCl), 1-dodecyl-3-methylimidazolium chloride (C$_{12}$MIMCl), and polyethylene-polypropylene glycol (P123).

The adsorption kinetics of EIMS/NIMS for Cyt c are shown in Figure 5b. It can be seen that the adsorption equilibrium can be achieved within 10 min for both microspheres. Then, the pseudo-first-order and pseudo-second-order kinetic models are applied to investigate the controlling mechanism of the binding process (Table 3, eqs S3 and S4).[43,44] In general, the pseudo-first-order model supposes that the adsorption process is based on physical adsorption, whereas the pseudo-second-order model assumes that the adsorption rate is governed by chemical adsorption.[45] According to the correlation coefficient (R^2) value, the pseudo-second-order kinetic model better fits the binding process of EIMS for Cyt c, demonstrating that Cyt c can complementarily match the imprinted sites via multiple interactions to achieve fast, efficient, and accurate adsorption. In contrast to the EIMS, the quasi-first-order kinetic equation better fits NIMS, which indicates that the physical adsorption is dominated. That is to say, specific adsorption only occurs at the imprinting cavities other than polymer network or randomly distributed monomers.

3.4. Selectivity Study. To confirm the high specificity of EIMS toward the target protein Cyt c, we compared the adsorption performance to other proteins with similar IEPs or molecular weight (BSA, BHb, Lyz, and OVA). The adsorption experiments of different proteins were conducted in a single buffer solution (pH = 7.4) with a concentration of 1.8 mg

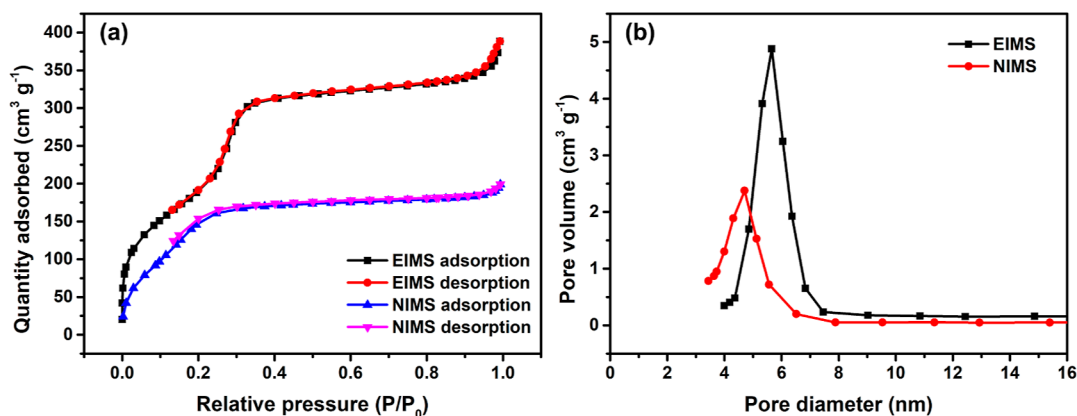**Figure 4.** (a) Nitrogen adsorption−desorption isotherms; (b) pore size distribution for EIMS and NIMS.
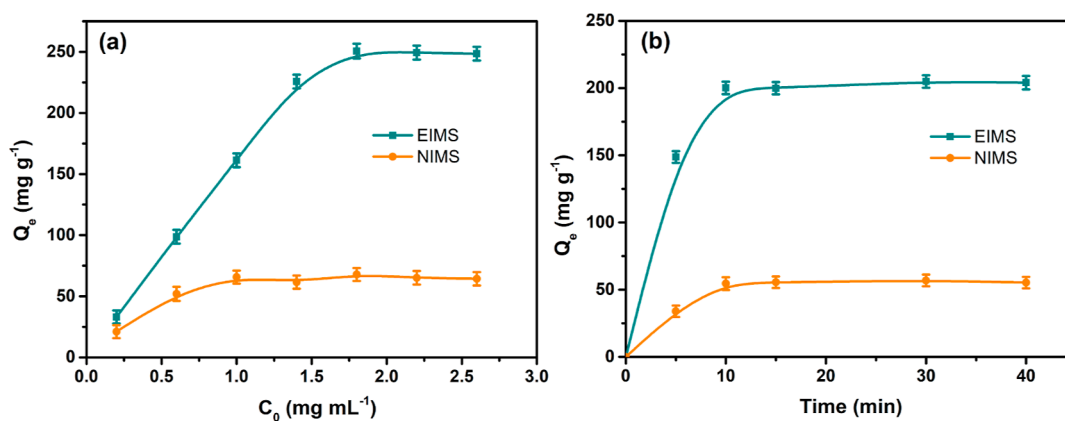
Figure 5. (a) Adsorption isotherm of Cyt *c* on EIMS and NIMS; (b) adsorption dynamic curves of Cyt *c* on EIMS and NIMS EIMS/NIMS.

Table 2. Isotherm Constants for Cyt *c* Adsorption onto EIMS and NIMS

isotherm model	Langmuir			Freundlich		
materials	Q_{max} (mg g^{-1})	K_L (L·mg^{-1})	R^2	K_F (mg g^{-1})	n	R^2
EIMS	448.3	0.5826	0.9596	156.8	1.6486	0.9198
NIMS	78.8	2.7494	0.9134	54.1	3.3584	0.7605

Table 3. Fitting Parameters of the Pseudo-First-Order and Pseudo-Second-Order

kinetic model	pseudo-first-order				pseudo-second-order		
materials	Q_e (mg g^{-1})	$Q_{e,c}$ (mg g^{-1})	k_1 (min^{-1})	R^2	$Q_{e,c}$ (mg g^{-1})	k_2 (g mg^{-1} min^{-1})	R^2
EIMS	249.6	254.0	0.2436	0.9764	277.63	0.0015	0.9919
NIMS	65.6	66.9	0.2367	0.9935	73.38	0.0054	0.9785

mL^{-1}. As shown in Figure 6, the adsorption capacity of EIMS toward Cyt *c* is much better than that of other proteins, and
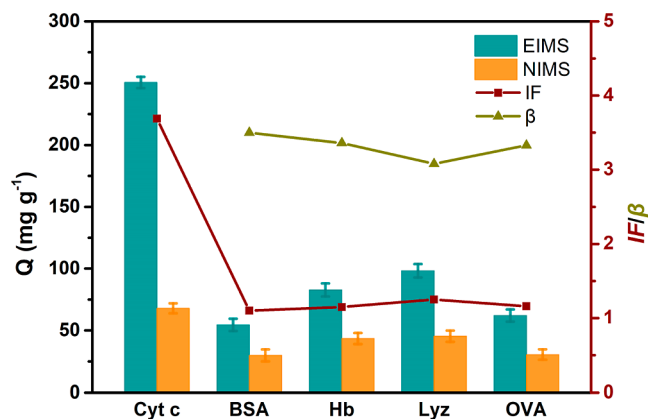

Figure 6. Specific recognition performance of EIMS.

the IF (IF$_{Cyt\ c}$) reaches 3.86 which is higher than that of the reference proteins (IF$_{BSA}$ = 1.10, IF$_{Hb}$ = 1.15, IF$_{Lyz}$ = 1.25, IF$_{OVA}$ = 1.16). Correspondingly, the selectivity coefficient (β) declares that the specific recognition ability of EIMS to Cyt *c* is 3.50, 3.36, 3.08, and 3.33 times higher than that of BSA, Hb, Lyz, and OVA, respectively. For BSA, Hb and OVA, low adsorption capacities of EIMS are attributed to electrostatic repulsion between EIMS and these comparative proteins by referring to their isoelectric points. For Lyz which is most close to Cyt *c* in terms of isoelectric point and molecular weight, the same low adsorption capacity and selectivity indicates the successful generation of imprinting cavities, which well match

the shape and functional groups of Cyt *c* other than analogues when using the characteristic nonapeptide fragment of Cyt *c* as the template.

3.5. Competitive Adsorption Performance. The competitive adsorption performance of EIMS for Cyt *c* was studied in a mixed solution of Cyt *c* and BSA as a competing molecule, and the results are shown in Figure 7 and Table 4. In the process of competitive recognition adsorption, both EIMS and NIMS show different adsorption capacities for Cyt *c* and BSA. However, the adsorption capacity of Cyt *c* ($Q_{Cyt\ c}$) by EIMS was not only significantly higher than that of BSA (Q_{BSA}) but also significantly higher than the $Q_{Cyt\ c}$ of NIMS. In addition, the selective recognition and adsorption of Cyt *c* by
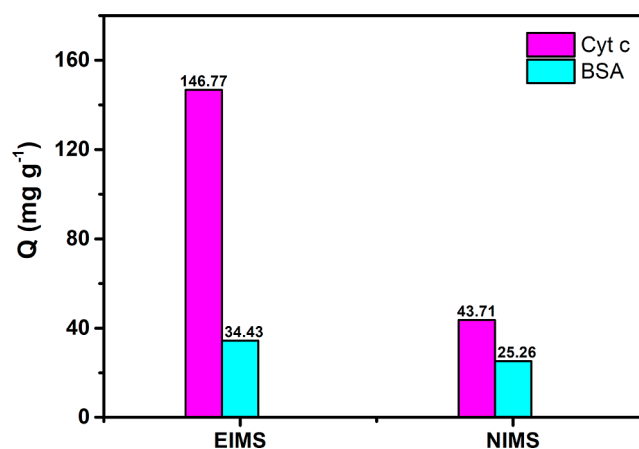

Figure 7. Adsorption capacity of Cyt *c* and BSA by EIMS and NIMS in a mixed solution.

Table 4. Adsorbing Capacity and $\alpha_{\text{Cyt c/BSA}}$ of EIMS and NIMS in a Mixed Solution

materials	$Q_{\text{Cyt c}}$ (mg g^{-1})	Q_{BSA} (mg g^{-1})	$\alpha_{\text{Cyt c/BSA}}$
EIMS	146.77	34.43	4.26
NIMS	43.71	25.26	1.73

EIMS is significantly better than that by NIMS. The recognition factor of Cyt c ($\alpha_{\text{Cyt c/BSA}}$) for EIMS in mixed solution was 4.26, which was significantly higher than the $\alpha_{\text{Cyt c/BSA}}$ of NIMS with a value of 1.73. Besides, as described above, the equilibrium adsorption amount of EIMS for Cyt c shows certain superiority when compared with other results in the reported literature, as shown in Table 5.[46−49] Therefore, it can be concluded that EIMS has the ability to select and recognize Cyt c efficiently and accurately in a mixed solution of proteins.

Table 5. Comparison of Different Methods of Imprinting Cyt c

carrier	imprinting strategies	Q_e (mg g^{-1})	adsorption rate	IF	ref
Fe$_3$O$_4$	surface imprinting	70.23	15 min	2.99	46
organic polymers	protein imprinting	67.4	4 h	3.19	47
cryogel	protein imprinting	98.33		5.36	48
hydrogels	protein imprinting	78		2.60	49
Fe$_3$O$_4$@SiO$_2$	epitope imprinting	67.6	2 h	4.54	11
mesoporous silica	epitope imprinting	86.5	20 min	3.48	25
mesoporous silica	epitope imprinting	250.6	10 min	3.86	this method

3.6. Adsorption Performance in Real Sample. In order to verify the selective adsorption performance of BIMS in real samples, the adsorption experiments of BIMS and NIMS in real fetal bovine serum (FCS) samples were carried out, and SDS−PAGE results are shown in Figure 8. FCS contains a variety of proteins (column 2), and a very dark band appears at 66.2 kDa as the standard protein electrophoretic band (column 1), indicating a higher concentration of BSA. Proteins eluted from the EIMs (column 4) show electrophoretic bands at the location at 14.4 kDa. These results indicate the selective adsorption performance of BIMS in real samples.

3.7. Reusability Performance. Reusability is one of the vital criteria to evaluate the practical applications of imprinted materials. Therefore, we investigate the reuse performance of EIMS and NIMS through adsorption−desorption 10 cycles in Cyt c solution (pH = 7.4) with a concentration of 1.8 mg·mL^{-1}. As shown in Figure 9, the adsorption amount (Q) of EIMS for Cyt c progressively decreases by 10% after seven adsorption−desorption cycles. The decrease in the adsorption capacity of EIMS for Cyt c may be due to some adsorption sites in the mesopores of EIMS being blocked or destroyed during the adsorption−desorption procedure. Besides, the adsorption amount of EIMS for Cyt c is 226.60 mg g^{-1} after five cycles, which is much higher than that of NIMs for Cyt c with a value of 53.48 mg g^{-1}. Comparing the reusabilities of EIMS with other reported works in Table S1, EIMS shows satisfactory reusability, and it still has good specific adsorption
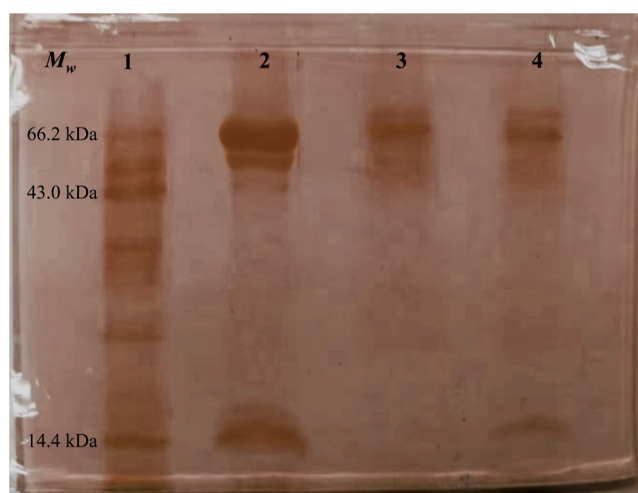

Figure 8. SDS−PAGE results of competition experiment (lane 1, protein molecular weight marker; lane 2, PBS diluent of FCS samples and Cyt c; lane 3, proteins eluted from NIMS; and lane 4, proteins eluted from EIMS).
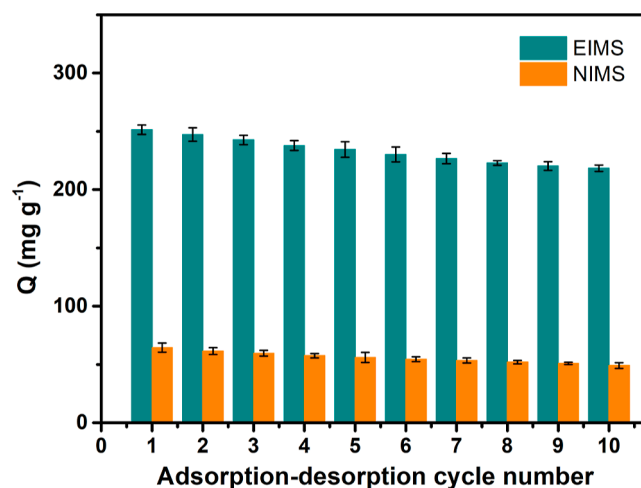

Figure 9. Reusabilities of EIMS and NIMS.

ability and adsorption capacity after multiple adsorption−desorption cycles.[46,48,50−52]

4. CONCLUSIONS

In summary, EIMS displays high adsorption capacity (250.6 mg g^{-1}) and fast adsorption equilibrium (10 min), as well as excellent specificity toward Cyt c. The introduction of amphiphilic ILs could well anchor templates via multiple interactions. The presence of organic auxiliaries in amphiphilic ILs significantly enhance the saturated adsorption capacity and equilibrium rate. The imprinted cavities located on the surface of mesoporous channels allow Cyt c to specifically bind to the numerous imprinted sites with high accessibility and easy mass transfer. Thus, this novel approach composed of epitope templates and docking oriented imprinting holds great potential for efficient separation and recognition of proteins.

■ ASSOCIATED CONTENT

ⓢ Supporting Information

The Supporting Information is available free of charge at https://pubs.acs.org/doi/10.1021/acsomega.3c07387.

FTIR spectra of C$_{16}$MIMCl and the corresponding description; ^{1}H NMR spectrum of C$_{16}$MIMCl and the corresponding description; Langmuir isotherm model and Freundlich isotherm model; quasi-first-order kinetic equation and quasi-second-order kinetic equation; and adsorption capacity for different imprinted materials after multiple cycles (PDF)

■ AUTHOR INFORMATION

Corresponding Author

Yan Li − National Local Joint Engineering Research Center for Precision Surgery & Regenerative Medicine, First Affiliated Hospital of Xi'an Jiaotong University, Xi'an 710061, P. R. China; ⓞ orcid.org/0009-0003-6727-8808; Email: liy9869@xjtu.edu.cn

Authors

Dandan Cheng − School of Life Science, Wuchang University of Technology, Wuchang, Wuhan 430223, P. R. China; ⓞ orcid.org/0009-0000-5882-4895

Xin Han − The Key Laboratory of Space Applied Physics and Chemistry, School of Chemistry and Chemical Engineering, Northwestern Polytechnical University, Xi'an 710129, P. R. China

Jiawen Zou − School of Life Science, Wuchang University of Technology, Wuchang, Wuhan 430223, P. R. China

Zhenyu Li − Xi'an Jiaotong University Health Science Center, Xi'an 710061, P. R. China

Meiru Wang − Xi'an Jiaotong University Health Science Center, Xi'an 710061, P. R. China

Yuqing Liu − Xi'an Jiaotong University Health Science Center, Xi'an 710061, P. R. China

Kexuan Wang − Xi'an Jiaotong University Health Science Center, Xi'an 710061, P. R. China

Complete contact information is available at:
https://pubs.acs.org/10.1021/acsomega.3c07387

Author Contributions

Dandan Cheng and Xin Han contributed equally to this work. Dandan Cheng: conceptualization, methodology, writing— original draft, and writing—review and editing. Xin Han: methodology and writing—original draft. Jiawen Zou: visualization. Zhenyu Li: data curation. Meiru Wang: resources. Yuqing Liu: formal analysis. Kexuan Wang: investigation. Yan Li: project administration and funding acquisition.

Funding

Notes

The authors declare no competing financial interest.

■ REFERENCES

(1) Ostovan, A.; Arabi, M.; Wang, Y.; Li, J.; Li, B.; Wang, X.; Chen, L. Greenificated Molecularly Imprinted Materials for Advanced Applications. *Adv. Mater.* **2022**, *34*, 2203154.

(2) Zhang, N.; Zhang, N.; Xu, Y. R.; Li, Z. L.; Yan, C. R.; Mei, K.; Ding, M.; Ding, S.; Guan, P.; Qian, L.; et al. Molecularly imprinted materials for selective biological recognition. *Macromol. Rapid Commun.* **2019**, *40*, No. e1900096.

(3) Mustafa, Y. L.; Keirouz, A.; Leese, H. S. Molecularly imprinted polymers in diagnostics: accessing analytes in biofluids. *J. Mater. Chem. B* **2022**, *10*, 7418−7449.

(4) Xing, R.; Wen, Y.; He, H.; Guo, Z.; Liu, Z. Recent progress in the combination of molecularly imprinted polymer-based affinity extraction and mass spectrometry for targeted proteomic analysis. *TrAC, Trends Anal. Chem.* **2019**, *110*, 417−428.

(5) Wang, M.; Zhou, J.; Zhang, G.; Liu, Q.; Zhang, Q. Pyrrolidinyl ligand motif-assisted bovine serum albumin molecularly imprinted polymers with high specificity. *J. Colloid Interface Sci.* **2022**, *609*, 102− 113.

(6) Zhang, W.; Zhang, Y.; Wang, R.; Zhang, P.; Zhang, Y.; Randell, E.; Zhang, M.; Jia, Q. A review: Development and application of surface molecularly imprinted polymers toward amino acids, peptides, and proteins. *Anal. Chim. Acta* **2022**, *1234*, 340319.

(7) Ding, S.; Lyu, Z.; Niu, X.; Zhou, Y.; Liu, D.; Falahati, M.; Du, D.; Lin, Y. Integrating ionic liquids with molecular imprinting technology for biorecognition and biosensing: A review. *Biosens. Bioelectron.* **2020**, *149*, 111830.

(8) Khumsap, T.; Corpuz, A.; Nguyen, L. T. Epitope-imprinted polymers: applications in protein recognition and separation. *RSC Adv.* **2021**, *11*, 11403−11414.

(9) Luo, Y.; Song, Y.; Wang, M.; Jian, T.; Ding, S.; Mu, P.; Liao, Z.; Shi, Q.; Cai, X.; Jin, H.; Du, D.; Dong, W. J.; Chen, C. L.; Lin, Y. Bioinspired Peptoid Nanotubes for Targeted Tumor Cell Imaging and Chemo-Photodynamic Therapy. *Small* **2019**, *15*, No. e1902485.

(10) Nishino, H.; Huang, C.-S.; Shea, K. J. Selective Protein Capture by Epitope Imprinting. *Angew. Chem., Int. Ed.* **2006**, *45*, 2392−2396.

(11) Zhang, X.; Zhang, N.; Du, C.; Guan, P.; Gao, X.; Wang, C.; Du, Y.; Ding, S.; Hu, X. Preparation of magnetic epitope imprinted polymer microspheres using cyclodextrin-based ionic liquids as functional monomer for highly selective and effective enrichment of cytochrome c. *Chem. Eng. J.* **2017**, *317*, 988−998.

(12) Eguílaz, M.; Villalonga, R.; Rivas, G. Electrochemical biointerfaces based on carbon nanotubes-mesoporous silica hybrid material: Bioelectrocatalysis of hemoglobin and biosensing applications. *Biosens. Bioelectron.* **2018**, *111*, 144−151.

(13) Liu, X.; Zhang, F.; Jing, X.; Pan, M.; Liu, P.; Li, W.; Zhu, B.; Li, J.; Chen, H.; Wang, L.; Lin, J.; Liu, Y.; Zhao, D.; Yan, H.; Fan, C. Complex silica composite nanomaterials templated with DNA origami. *Nature* **2018**, *559*, 593−598.

(14) Manzano, M.; Vallet-Regí, M. Mesoporous Silica Nanoparticles for Drug Delivery. *Adv. Funct. Mater.* **2019**, *30*, 1902634.

(15) Croissant, J. G.; Fatieiev, Y.; Almalik, A.; Khashab, N. M. Mesoporous Silica and Organosilica Nanoparticles: Physical Chemistry, Biosafety, Delivery Strategies, and Biomedical Applications. *Adv. Healthcare Mater.* **2017**, *7*, 1700831.

(16) Gao, M.; Nakajima An, D.; Skolnick, J. Deep learning-driven insights into super protein complexes for outer membrane protein biogenesis in bacteria. *Elife* **2022**, *11*, No. e82885.

(17) Fan, J. P.; Yu, J. X.; Yang, X. M.; Zhang, X. H.; Yuan, T. T.; Peng, H. L. Preparation, characterization, and application of multiple stimuli-responsive rattle-type magnetic hollow molecular imprinted poly (ionic liquids) nanospheres (Fe$_3$O$_4$ @void@PILMIP) for specific recognition of protein. *Chem. Eng. J.* **2018**, *337*, 722−732.

(18) Zhou, P.; Li, X.; Zhou, J.; Li, W.; Shen, L. A molecular imprinting polymer based on computer-aided design: Selective enrichment and purification of synephrine from the extract waste liquid of Citrus aurantium L. *React. Funct. Polym.* **2023**, *190*, 105647.

(19) Du, C. B.; Hu, X. L.; Guan, P.; Gao, X. M.; Song, R. Y.; Li, J.; Qian, L. W.; Zhang, N.; Guo, L. X. Preparation of surface-imprinted

microspheres effectively controlled by orientated template immobilization using highly cross-linked raspberry-like microspheres for the selective recognition of an immunostimulating peptide. *J. Mater. Chem. B* **2016**, *4*, 1510−1519.

(20) Hazrati, N.; Beigi, A. A. M.; Abdouss, M. Demulsification of water in crude oil emulsion using long chain imidazolium ionic liquids and optimization of parameters. *Fuel* **2018**, *229*, 126−134.

(21) Atta, A. M.; Al-Lohedan, H. A.; Abdullah, M. M.; ElSaeed, S. M. Application of new amphiphilic ionic liquid based on ethoxylated octadecylammonium tosylate as demulsifier and petroleum crude oil spill dispersant. *J. Ind. Eng. Chem.* **2016**, *33*, 122−130.

(22) Wang, J.; Zhang, C.; Bai, Y.; Li, Q.; Yang, X. Synthesis of mesoporous silica with ionic liquid surfactant as template. *Mater. Lett.* **2021**, *291*, 129556.

(23) Costa, J. A. S.; Vedovello, P.; Paranhos, C. M. Use of Ionic Liquid as Template for Hydrothermal Synthesis of the MCM-41 Mesoporous Material. *Silicon* **2020**, *12*, 289−294.

(24) Ding, S. C.; Li, Z. L.; Cheng, Y.; Du, C. B.; Gao, J. F.; Zhang, Y. W.; Zhang, N.; Li, Z. T.; Chang, N.; Hu, X. Enhancing adsorption capacity while maintaining specific recognition performance of mesoporous silica: a novel imprinting strategy with amphiphilic ionic liquid as surfactant. *Nanotechnology* **2018**, *29*, 375604.

(25) Li, Z. L.; Guan, P.; Hu, X. L.; Ding, S. C.; Tian, Y.; Xu, Y. R.; Qian, L. W. Preparation of molecularly imprinted mesoporous materials for highly enhancing adsorption performance of cytochrome c. *Polymers* **2018**, *10*, 298.

(26) Gao, Y.; He, Y.; Zhang, H.; Zhang, Y.; Gao, T.; Wang, J.-H.; Wang, S. Zwitterion-functionalized mesoporous silica nanoparticles for enhancing oral delivery of protein drugs by overcoming multiple gastrointestinal barriers. *J. Colloid Interface Sci.* **2021**, *582*, 364−375.

(27) Zhang, Z.; Li, J. H.; Wang, X. Y.; Shen, D. Z.; Chen, L. X. Quantum dots based mesoporous structured imprinting microspheres for the sensitive fluorescent detection of phycocyanin. *ACS Appl. Mater. Interfaces* **2015**, *7*, 9118−9127.

(28) Dai, Y.; Yang, D.; Yu, D.; Xie, S.; Wang, B.; Bu, J.; Shen, B.; Feng, W.; Li, F. Engineering of monodisperse core−shell upconversion dendritic mesoporous silica nanocomposites with a tunable pore size. *Nanoscale* **2020**, *12*, 5075−5083.

(29) Wen, T.; Yuan, J.; Lai, W.; Liu, X.; Liu, Y.; Chen, L.; Jiang, X. Morphology-Controlled Mesopores with Hydrophilic Pore Walls from Triblock Copolymers. *Macromolecules* **2022**, *55* (11), 4812−4820.

(30) Liu, H.; He, J.; Zhu, K.; Zhu, D.; Zhu, L.; Zhu, W.; Li, H.; Jiang, W. Modification of cobalt doped mesoporous sieve by grafting N,N-dihydroxypyromellitimide to enhance desulfurization catalyst stability. *J. Mol. Liq.* **2023**, *390*, 122970.

(31) Wang, L.; Zhang, X.; Chen, X.; Li, X.; Zhao, Y.; Li, W.; Zhao, J.; Chen, Z.; Li, Y. A large-area, flexible, high contrast and long-life stable solid-state electrochromic device driven by an anion-assisted method. *J. Mater. Chem. C* **2021**, *9*, 1641−1648.

(32) Wu, D.; Yao, B.; Wu, S.; Hingorani, H.; Cui, Q.; Hua, M.; Frenkel, I.; Du, Y.; Hsiai, T. K.; He, X. Room-Temperature Annealing-Free Gold Printing via Anion-Assisted Photochemical Deposition. *Adv. Mater.* **2022**, *34*, 2201772.

(33) Zhao, W. K.; Sun, B. C.; Han, C. B.; Zhou, K. L.; Wang, C.; Zheng, J. Y.; Lu, Y.; Fang, D.; Yan, H. Anion assisted completely reconfigured manganese oxides with optimal proton adsorption for boosting acidic hydrogen evolution reaction. *Chem. Eng. J.* **2023**, *465*, 143006.

(34) Xie, Y.; Cheng, G.; Wu, Z.; Shi, S.; Zhao, J.; Jiang, L.; Jiang, D.; Yuan, M.; Wang, Y.; Yuan, M. Preparation and Characterization of New Electrospun Poly(lactic acid) Nanofiber Antioxidative Active Packaging Films Containing MCM-41 Mesoporous Molecular Sieve Loaded with Phloridzin and Their Application in Strawberry Packaging. *Nanomaterials* **2022**, *12* (7), 1229.

(35) Wang, C.-Y.; Lou, X.-Y.; Cai, Z.; Zhang, M.-Z.; Jia, C.; Qin, J.-C.; Yang, Y.-W. Supramolecular Nanoplatform Based on Mesoporous Silica Nanocarriers and Pillararene Nanogates for Fungus Control. *ACS Appl. Mater. Interfaces* **2021**, *13*, 32295−32306.

(36) Xu, C.; Lei, C.; Wang, Y.; Yu, C. Dendritic Mesoporous Nanoparticles: Structure, Synthesis and Properties. *Angew. Chem* **2022**, *134*, No. e202112752.

(37) Saini, K.; Prabhuraj, R. S.; Bandyopadhyaya, R. Development of Mesoporous Silica Nanoparticles of Tunable Pore Diameter for Superior Gemcitabine Drug Delivery in Pancreatic Cancer Cells. *J. Nanosci. Nanotechnol.* **2020**, *20*, 3084−3096.

(38) Karrat, A.; Lamaoui, A.; Arduini, F.; Amine, A. Ultrasound-Assisted Synthesis of an Advanced Sorbent Based on Amphiphilic Poly(Methacrylic Acid-co-Styrene) Modified Magnetic Nanoparticles for Removal and Analytical Determination of Dicofol. *Chem. Afr.* **2023**, *6*, 221−232.

(39) Zhao, W.; Li, B.; Xu, S.; Huang, X.; Luo, J.; Zhu, Y.; Liu, X. Electrochemical protein recognition based on macromolecular self-assembly of molecularly imprinted polymer: a new strategy to mimic antibody for label-free biosensing. *J. Mater. Chem. B* **2019**, *7*, 2311−2319.

(40) Chen, Y.; Li, X.; Yin, D.; Li, D.; Bie, Z.; Liu, Z. Dual-template docking oriented molecular imprinting: a facile strategy for highly efficient imprinting within mesoporous materials. *Chem. Commun.* **2015**, *51*, 10929−10932.

(41) Geng, Y.; Guo, M.; Tan, J.; Huang, S.; Tang, Y.; Tan, L.; Liang, Y. The fabrication of highly ordered fluorescent molecularly imprinted mesoporous microspheres for the selective sensing of sparfloxacin in biological samples. *Sens. Actuators, B* **2019**, *281*, 821−829.

(42) Shi, H.; Wang, Y.; Tang, C.; Wang, W.; Liu, M.; Zhao, G. Mechanisim investigation on the enhanced and selective photo-electrochemical oxidation of atrazine on molecular imprinted mesoporous TiO_2. *Appl. Catal., B* **2019**, *246*, 50−60.

(43) Du, C.; Hu, X.; Cheng, Y.; Gao, J.; Zhang, Y.-W.; Su, K.; Li, Z.; Zhang, N.; Chang, N.; Zeng, K. Synergetically understanding the interaction between nano/microspheres and peptide for controllable drug loading via experimental and theoretical approaches. *Mater. Sci. Eng., C* **2018**, *83*, 169−176.

(44) Fan, J.-P.; Dong, W.-Y.; Zhang, X.-H.; Yu, J.-X.; Huang, C.-B.; Deng, L.-J.; Chen, H.-P.; Peng, H.-L. Preparation and Characterization of Protein Molecularly Imprinted Poly (Ionic Liquid)/Calcium Alginate Composite Cryogel Membrane with High Mechanical Strength for the Separation of Bovine Serum Albumin. *Molecules* **2022**, *27* (21), 7304.

(45) Gao, X.; Hu, X.; Guan, P.; Du, C.; Ding, S.; Zhang, X.; Li, B.; Wei, X.; Song, R. Synthesis of core−shell imprinting polymers with uniform thin imprinting layer via iniferter-induced radical polymerization for the selective recognition of thymopentin in aqueous solution. *RSC Adv.* **2016**, *6*, 110019−110031.

(46) Wang, Y.; Xu, Y.; Gao, R.; Tian, X.; Heinlein, J.; Hussain, S.; Pfefferle, L. D.; Chen, X.; Zhang, X.; Hao, Y. Strategic design and fabrication of lightweight sesame ball-like hollow double-layer hybrid magnetic molecularly imprinted nanomaterials for the highly specific separation and recovery of tetracycline from milk. *Green Chem.* **2022**, *24*, 8036−8045.

(47) Guo, T.; Deng, Q.; Fang, G.; Liu, C.; Huang, X.; Wang, S. Molecularly imprinted upconversion nanoparticles for highly selective and sensitive sensing of Cytochrome c. *Biosens. Bioelectron.* **2015**, *74*, 498−503.

(48) Canpolat, G.; Dolak, İ.; Onat, R.; Keçili, R.; Baysal, Z.; Ziyadanoğulları, B.; Ersöz, A.; Say, R. Development of molecular imprinting-based smart cryogels for selective recognition and separation of serum cytochrome-c as a biochemical indicator. *Process Biochem.* **2021**, *106*, 112−119.

(49) Kubo, T.; Arimura, S.; Tominaga, Y.; Naito, T.; Hosoya, K.; Otsuka, K. Molecularly Imprinted Polymers for Selective Adsorption of Lysozyme and Cytochrome c Using a PEG-Based Hydrogel: Selective Recognition for Different Conformations Due to pH Conditions. *Macromolecules* **2015**, *48*, 4081−4087.

(50) Shah, S. A. H.; Ramachandran, M. R.; Mansur, S. A.; Saleh, N. M.; Asman, S. Selective recognition of bisphenol a using molecularly imprinted polymer based on choline chloride-methacrylic acid deep

eutectic solvent monomer: Synthesis characterization and adsorption study. *Polymer* **2023**, *283*, 126279.

(51) Lu, J.; Qin, Y.; Wu, Y.; Meng, M.; Dong, Z.; Yu, C.; Yan, Y.; Li, C.; Nyarko, F. K. Bidirectional molecularly imprinted membranes for selective recognition and separation of pyrimethamine: A double-faced loading strategy. *J. Membr. Sci.* **2020**, *601*, 117917.

(52) Mandani, S.; Rezaei, B.; Ensafi, A. A. Sensitive imprinted optical sensor based on mesoporous structure and green nanoparticles for the detection of methamphetamine in plasma and urine. *Spectrochim. Acta, Part A* **2020**, *231*, 118077.